Talanta 129 (2014) 55–62

Contents lists available at ScienceDirect

Talanta

journal homepage: www.elsevier.com/locate/talanta

Metal organic frameworks/macroporous carbon composites with enhanced stability properties and good electrocatalytic ability for ascorbic acid and hemoglobin

Yufan Zhang, Anaclet Nsabimana, Liande Zhu, Xiangjie Bo, Ce Han, Mian Li, Liping Guo *

Faculty of Chemistry, Northeast Normal University, 130024 Changchun, PR China

ARTICLE INFO

Article history:
Received 26 January 2014
Received in revised form
29 April 2014
Accepted 5 May 2014
Available online 22 May 2014

Keywords:
Thermal
Water and electrochemical stability
Metal organic frameworks
Macroporous carbon
Electrochemical sensors

ABSTRACT

The thermal, water and electrochemical stability of Cu-based metal organic frameworks (Cu-MOFs) confined in macroporous carbon (MPC) hybrids has been investigated. Thermogravimetric analyses, X-Ray diffraction, scanning electron microscopy, and cyclic voltammetry were employed to confirm the stability of pure Cu-MOFs, MPC, and Cu-MOFs-MPC. As compared to pure Cu-MOFs, the porous composite materials of MPC and Cu-MOFs interact and seem to form new materials having homogenous structure and chemistry, which show structural stability in aqueous media and electrochemical stability in phosphate buffer solution (PBS pH 7.4). The detection of ascorbic acid and hemoglobin is performed as an electrochemical probe, indicating Cu-MOFs-MPC holds great promise for the design of electrochemical sensors.

1. Introduction

Metal organic frameworks (MOFs) have many exciting characteristics including structural adaptivity and flexibility, ordered crystalline pores, and multiple coordination sites. There are an enormous number of MOFs that can be synthesized with various combinations of organic linkers and metal centers, providing an opportunity to tailor surface area, pore size, and surface functionality [1,2]. MOFs have become a leading class of porous materials for applications, such as gas storage or separation, drug delivery, optoelectronics, imaging, heterogeneous catalysis and even toxic gas removal [3–8]. In addition, the investigation of MOFs in electrochemical area is quite recent but expanding (e.g. electrode materials for batteries [9,10], electrocatalysts for oxygen reduction reaction [11], electrode materials for supercapacitors [12,13], and so on [14–17]). This is due to the redox behavior of metal cations inside MOFs which could provide a pathway for electrons. Alternatively, the tuning of the linker structure may lead to better charge transfer inside the framework. Importantly, the large majority of electrochemical reactions are occurring in aqueous phase. Yet, one of the major shortcomings of several classes of MOFs is their instability in the presence of moisture. This is because the entire framework of MOFs is supported by coordination bonds and/or other weak cooperative interactions such as H-bonding, π–π stacking, and van der Waals interaction. Thus, structural flexibility is often occurring easily even under mild conditions. The poor water stability gives rise to the framework collapse of the MOFs, even leading to the electrochemical instability [18]. Although some water-stable MOFs have emerged recently [19–21], the other current issue with implementing many types of MOFs into practical electrochemical applications is their weak conductivity. Therefore, the single-phase MOFs are still limited in electrochemical performance because of their intrinsic weaker material properties such as electronic conductivity, water and electrochemical stability. Based on these considerations, heterogeneous nanostructured materials with multi-nanocomponents have attracted our attention. An efficient strategy is to mix MOFs with conductive phases (metal nanocrystals, carbon nanostructures, conductive polymers, etc.) [22–24]. This will provide electron conduction at a macroscopic level. Recently, our group has still studied the MOFs–carbon combination composites. In the previous study, we reported the easy preparation of novel Cu-based MOFs loaded on macroporous carbon (MPC) hybrids [25]. Through the analyses of the characterization and electrochemical experiments, we found that the nano-sized and nanocrystalline novel material has greatly improved electronic conductivity and enhanced electrocatalytic ability. In this communication, the thermal, water and electrochemical stability of the pure Cu-MOFs and Cu-MOFs-MPC composite was investigated and discussed in detail for the first time. More importantly, the Cu-MOFs-MPC exhibits significant catalytic activity for biomolecules

* Corresponding author. Tel./fax: +86 431 85099762.
E-mail address: guolp078@nenu.edu.cn (L. Guo).

http://dx.doi.org/10.1016/j.talanta.2014.05.007
0039-9140/

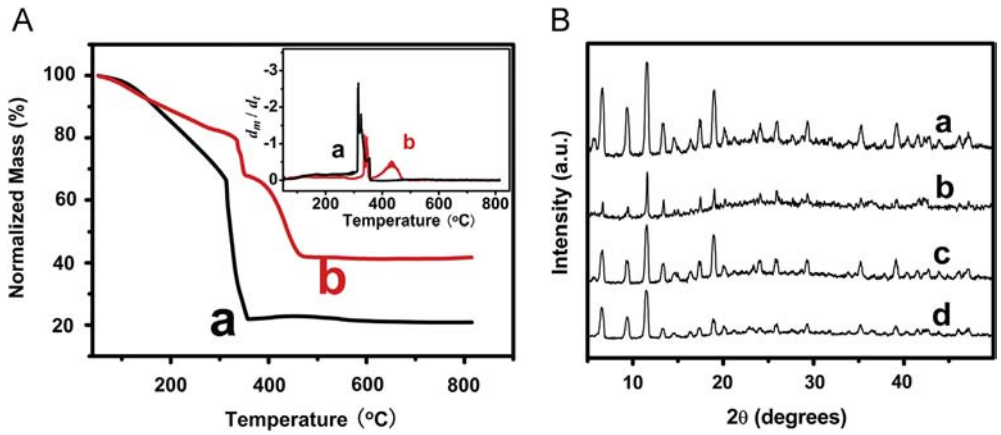

Fig. 1. (A) TGA and DTG (inset of Fig. 1A) curves of Cu-MOFs (a) and Cu-MOFs-MPC (b) at air atmosphere. (B) XRD patterns of Cu-MOFs before (a) and after (b), Cu-MOFs-MPC before (c) and after (d) immersion in water.

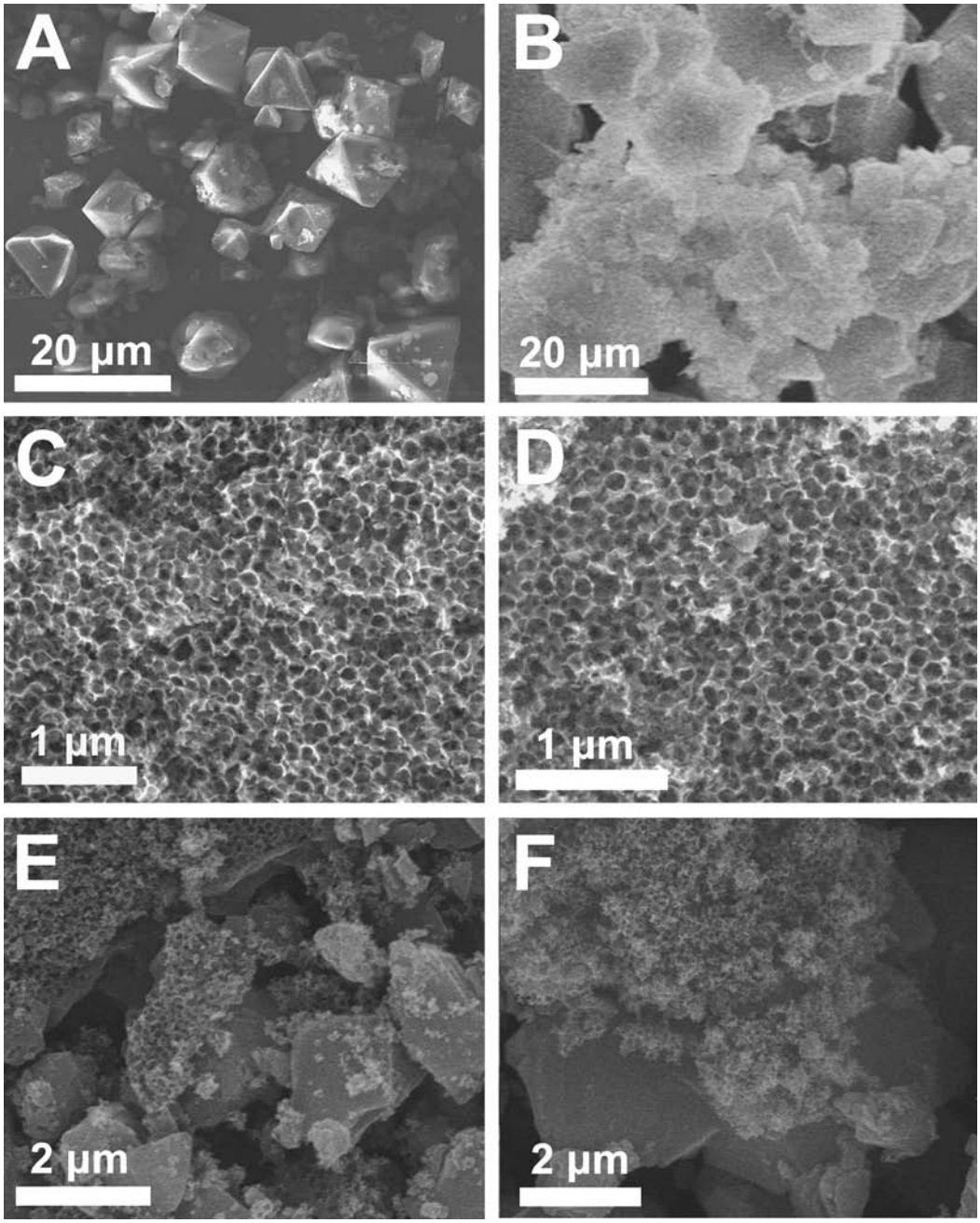

Fig. 2. SEM images of pure Cu-MOFs (A and B), MPC (C and D), and Cu-MOFs-MPC (E and F). (A), (C), and (E) are before and (B), (D), and (F) are after being exposed to water.

(ascorbic acid (AA) and hemoglobin (Hb)) in neutral solution (pH=7.4).

2. Experimental

2.1. Reagents and apparatus

N,N′-dimethylformamide (DMF) (HPLC grade), 1,3,5-benzenetricarboxylic acid (H_3BTC) and $Cu(NO_3)_2 \cdot 3H_2O$ were used as purchased from Beijing Chemical Co., Ltd. AA and Hb were obtained from Sigma. The 0.1 M phosphate buffer solution (PBS pH 7.4), which was made up from NaH_2PO_4, Na_2HPO_4, and H_3PO_4, was employed as a supporting electrolyte. All other reagents were of analytical grade, and all solutions were prepared with double distilled water. All the electrochemical experiments were performed with a CHI 830B electrochemical Analyzer (CH Instruments, Shanghai Chenhua Instrument Corporation, China). A conventional three electrode cell was used; the used working electrode was glassy carbon electrode (GCE) or the modified electrode; a platinum electrode was applied as the counter-electrode and an Ag/AgCl (in saturated KCl solution) electrode served as a reference electrode. In this study, all the sample solutions were purged with purified nitrogen for 20 min to remove oxygen prior to the beginning of a series of experiments and all experiments were carried out at laboratory temperature. Scanning electron microscopy (SEM) images were determined with a Philips XL-30 ESEM operating at 3.0 kV. Thermogravimetric analysis (TGA) was performed on a PerkinElmer Diamond TG Analyzer. X-Ray diffraction (XRD) patterns were obtained on an X-Ray D/max-2200vpc (Rigaku Corporation, Japan) instrument operated at 40 kV and 20 mA using Cu Kα radiation (k=0.15406 nm).

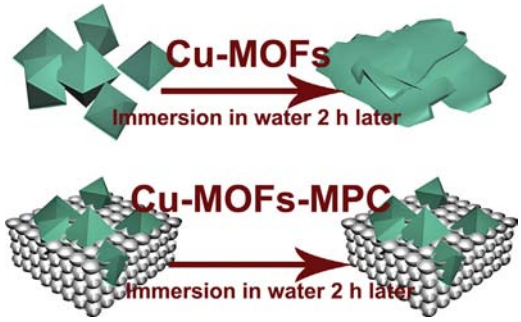

Fig. 3. Scheme of changes in morphology after the immersion of Cu-MOFs and Cu-MOFs-MPC hybrids in water for 2 h.

2.2. Synthesis of Cu-MOFs and Cu-MOFs-MPC

The MPC was synthesized as in our previous report [26]. In a typical synthesis, the SiO_2 template was prepared by the typical Stober's method [27]. Carbon was introduced into the interstices of the template using the modified method of Jun et al. [28]. In a typical synthesis, 2.0 g of sucrose was dissolved in 10 mL aqueous solution containing 0.15 mL of 98% H_2SO_4. 2.0 g of SiO_2 template was immersed into sucrose solution and kept in vacuum for 3 h at room temperature for thorough impregnation. Then the mixture was heated at 100 °C for 6 h, followed by heating at 160 °C for a further 6 h for polymerization of sucrose. The solid was subsequently carbonized at 900 °C in N_2 for 3 h in a tube oven. The SiO_2 template was then etched away by overnight dissolution in 10% aqueous HF to leave behind a MPC.

The Cu-MOFs and Cu-MOFs-MPC were prepared like we previously reported [25]. In a typical synthesis, 87.5 mg (3.6 mmol) $Cu(NO_3)_2 \cdot 3H_2O$ were dissolved in 12 mL DMF and mixed with 42 mg (2.0 mmol) of H_3BTC dissolved in 12 mL ethanol. The solution was filled in a 40 mL Teflon liner, placed in an autoclave, and heated to 120 °C for 12 h. The obtained blue powder was recovered by filtration, and then washed with DMF. Thereafter, the Cu-MOFs

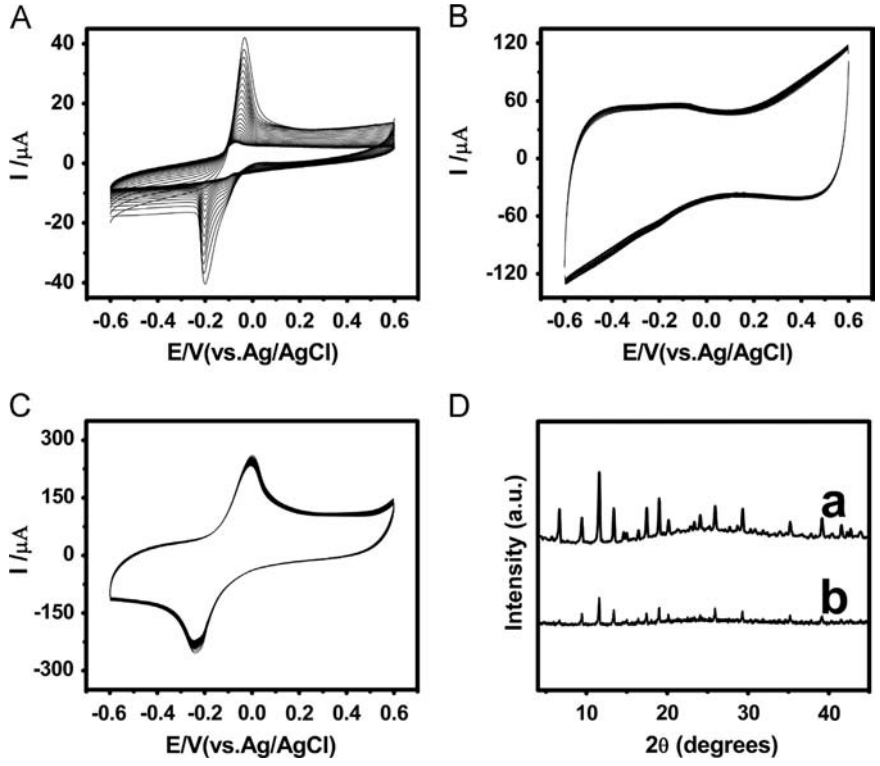

Fig. 4. CV experiments (30 cycles) of pure Cu-MOFs (A), MPC (B), and Cu-MOFs-MPC (C) in 0.10 M PBS (pH=7.4). Scan rate: 50 mV s^{-1}. (D) XRD patterns of Cu-MOFs-MPC (a) and Cu-MOFs (b) after successive CV scans.

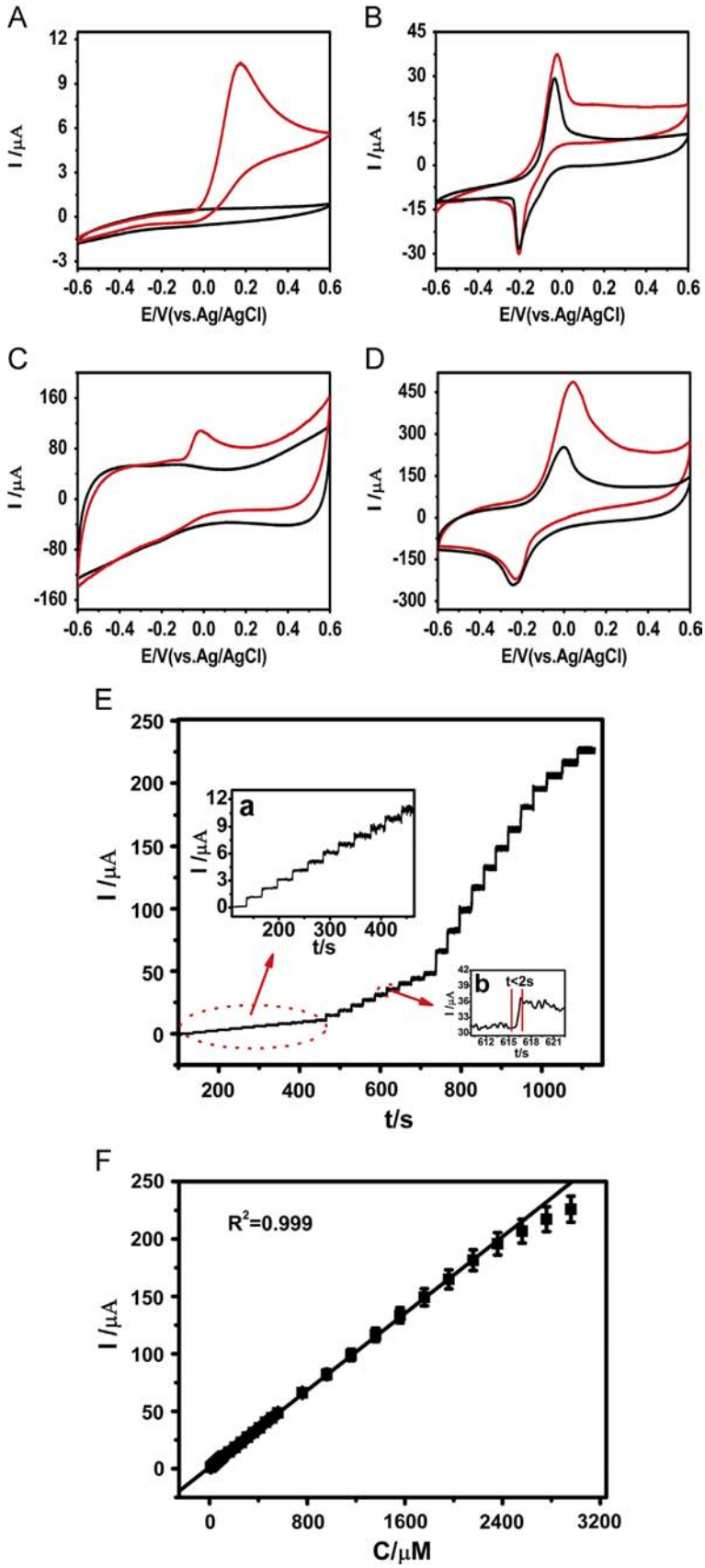

Fig. 5. CVs of bare GCE (A), Cu-MOF/GCE (B), MPC/GCE (C), and Cu-MOF-MPC/GCE (D) in the absence (black line) and presence (red line) of 0.5 mM AA in (pH=7.4). Scan rate: 50 mV s^{-1}. Starting potentials: −0.6 V. (E) Typical amperometric current–time curve of Cu-MOF–MPC/GCE with successive additions of AA. Inset a: the amperometric response with successive addition of AA at lower concentration. Inset b: the current response time after the AA addition at Cu-MOF-MPC/GCE. (F) The linear dependence of between AA concentration and current signal for Cu-MOF-MPC/GCE. (For interpretation of the references to color in this figure legend, the reader is referred to the web version of this article.)

were obtained by vacuum drying at 80 °C. The Cu-MOFs-MPC composite materials were prepared by dispersing 518 mg of MPC powder (80 wt% of the final material) in the well-dissolved Cu $(NO_3)_2$/BTC mixture. The resulting suspensions were subsequently stirred and subjected to the same synthesis procedure as for Cu-MOFs.

2.3. Electrode preparation and modification

Prior to the modification, GCE (model CHI104, 3 mm diameter) was polished before each experiment with alumina power, and rinsed thoroughly with doubly distilled water between each polishing step. The cleaned electrode was dried with a high-purify nitrogen stream for the next modification. To prepare the modified electrodes, 5 mg of the as-prepared samples was dispersed into 1 mL DMF to give homogeneous suspension upon bath sonication. A 5 μL of the suspension was dip-coated onto GCE and the electrode was then dried at room temperature.

3. Results and discussion

3.1. Thermal, water and electrochemical stability of the as-prepared samples

To examine the thermal stability of the as-made pure Cu-MOFs and Cu-MOFs-MPC composites, TGA were carried out under an air atmosphere with a heating rate of 10 °C min^{-1} and the results are shown in Fig. 1A. In general, the TGA curve of the Cu-MOFs revealed two distinct weight loss steps corresponding to the loss of H_2O molecules, and to the decomposition of the organic linkers, respectively. As a comparison, the TGA curve of the Cu-MOFs-MPC showed three slightly and delayed weight losses, which are due to the encapsulation and protection effect of the carbon matrix. As can be seen from the inset of Fig. 1A, for pure Cu-MOFs sample, the intense endothermic–exothermal peaks in differential thermal analysis (DTG) curve between 305 and 340 °C were displayed, which are familiar with the Cu-MOFs-MPC in the temperature range of 335–360 °C due to the decomposition of Cu-MOFs crystallites. The results show the higher thermal stability of Cu-MOFs-MPC composites than that of pure Cu-MOFs crystallites.

The stability of Cu-MOFs and Cu-MOFs-MPC toward water was studied by XRD on samples exposed to aqueous conditions (Fig. 1B). The original Cu-MOFs (curve a) and Cu-MOFs-MPC (curve c) show clear reflections of the octahedral geometry of $Cu_3(BTC)_2$. Upon immersion in water at room temperature, the XRD pattern of pure Cu-MOFs completely changed over the period of 2 h (curve b), signifying major structural changes taking place. Interestingly, Cu-MOFs-MPC exhibits unchanged XRD patterns after two hours of immersion in water (curve d). The results indicate that water treatment gave no changes in the crystalline structure for Cu-MOFs-MPC.

SEM images of these synthetic materials before and after immersion in water were also acquired. In the image of the Cu-MOFs sample (Fig. 2A), the crystals of Cu-MOFs are clearly visible with truncated octahedral geometry and the crystallites of size varying between 10 and 20 μm, and are stacked together in an organized way. Unfortunately, after water treatment, the crystalline structure of Cu-MOFs has been changed (Fig. 2B). The big morphological change in the Cu-MOFs before and after water treatment implies the crystalline structure instability of Cu-MOFs in aqueous media. For MPC, the SEM images of MPC both are seen as well-defined interconnected macroporous nanostructure before (Fig. 2C) and after (Fig. 2D) being exposed to water, indicating the stability of MPC supports. Interestingly, as shown in Fig. 2E and F, the structural morphology of Cu-MOFs-MPC is almost unchanged after immersion in water, verifying the good stability of this Cu-MOFs-MPC in aqueous media. The scheme is shown in Fig. 3. These phenomena are consistent with XRD results. This happening may be due to two reasons: one is that the MPC skeleton exhibits a restriction effect on the growth of Cu-MOFs crystallites, and thus, the sizes of the crystallites match well with those of the macropores of the MPC matrix. This can largely decrease the size of crystalline structure. Another is that MPC seems to act as a strong support. The Cu-MOFs can be firmly fixed with MPC, so that the crystalline structure of Cu-MOF is stable.

To demonstrate the electrochemical stability of Cu-MOFs-MPC, cyclic voltammetry (CV) experiments (30 cycles) of Cu-MOFs, MPC, and Cu-MOFs-MPC in 0.10 M PBS (pH = 7.4) were performed. In Fig. 4A, the CVs of Cu-MOFs/GCE show one pair of redox wave at a formal potential of ca. −0.15 V, which was presumably ascribed to the redox process of $Cu^{II/I}$ in $Cu_2(BTC)_3$. Unfortunately, with the increase in the number of scan cycles, redox peak currents gradually decreased. The reduction current of Cu-MOFs is 28.5-fold larger than that of after 30 CV cycles. For MPC, the MPC/GCE was subjected to CV in aqueous solution and the current of MPC before and after 30 cycles CV scans show no changes (Fig. 4B). Surprisingly, for Cu-MOFs-MPC/GCE, redox peak current almost did not decrease after 30 CV cycles (Fig. 4C). After successive CV scans, XRD patterns of the Cu-MOFs-MPC were

Table 1
Comparison of the performance of the Cu-MOFs-MPC/GCE for the electrochemical detection of AA with that of other modified electrodes.

Working electrode	Potential (V)	Linear range (μM)	Sensitivity (μA mM^{-1})	Limit of detection (μM)	Reference
MCM-41/GCE[a]	0.14(SCE[b])	40–4000	48.36	10	[29]
MWCNT/GONR/GCE[c]	−0.035(SCE)	0.1–8.5	293.8	0.06	[30]
Graphene/Pt-modified GCE[d]	0.077 (Ag/AgCl)	0.15–34.4	345.7	0.15	[31]
PANI modified SPCE[e]	0.38 (SPCE)	30–270	17.7	30	[32]
poly-ACBK modified GCE[f]	0.12(Ag/AgCl)	50–1000	2	10	[33]
HNCMS/GC electrode[g]	0.08(SCE)	100–1000	27	0.91	[34]
SWCNH/GCE[h]	0(Ag/AgCl)	30–400	20	5	[35]
MWCNT-FeNAZ/GCE[i]	0.2(Ag/AgCl)	20–355	–	1.11	[36]
Cu-MOFs-MPC/GCE	0.04 (Ag/AgCl)	10–2360	83.64	3.5	This work

[a] A kind of mesoporous silica modified glassy carbon electrode.
[b] Saturated calomel electrode.
[c] A core–shell multiwalled carbon nanotubes/graphene oxide nanoribbons modified glassy carbon electrode.
[d] Graphene/Pt-modified glassy carbon electrode.
[e] Polyaniline modified Screen-Printed Carbon Electrode.
[f] A novel polymerized film of acid chrome blue K (ACBK) was prepared on the surface of a glassy carbon electrode.
[g] Phosphotungstate-doped glutaraldehydecross-linked poly-l-lysine film modified glassy carbon electrode.
[h] Single-walled carbon nanohorn modified glassy carbon electrode.
[i] Multiwall carbon nanotubes-iron ion-doped natrolite-chitosan modified glassy carbon electrode.

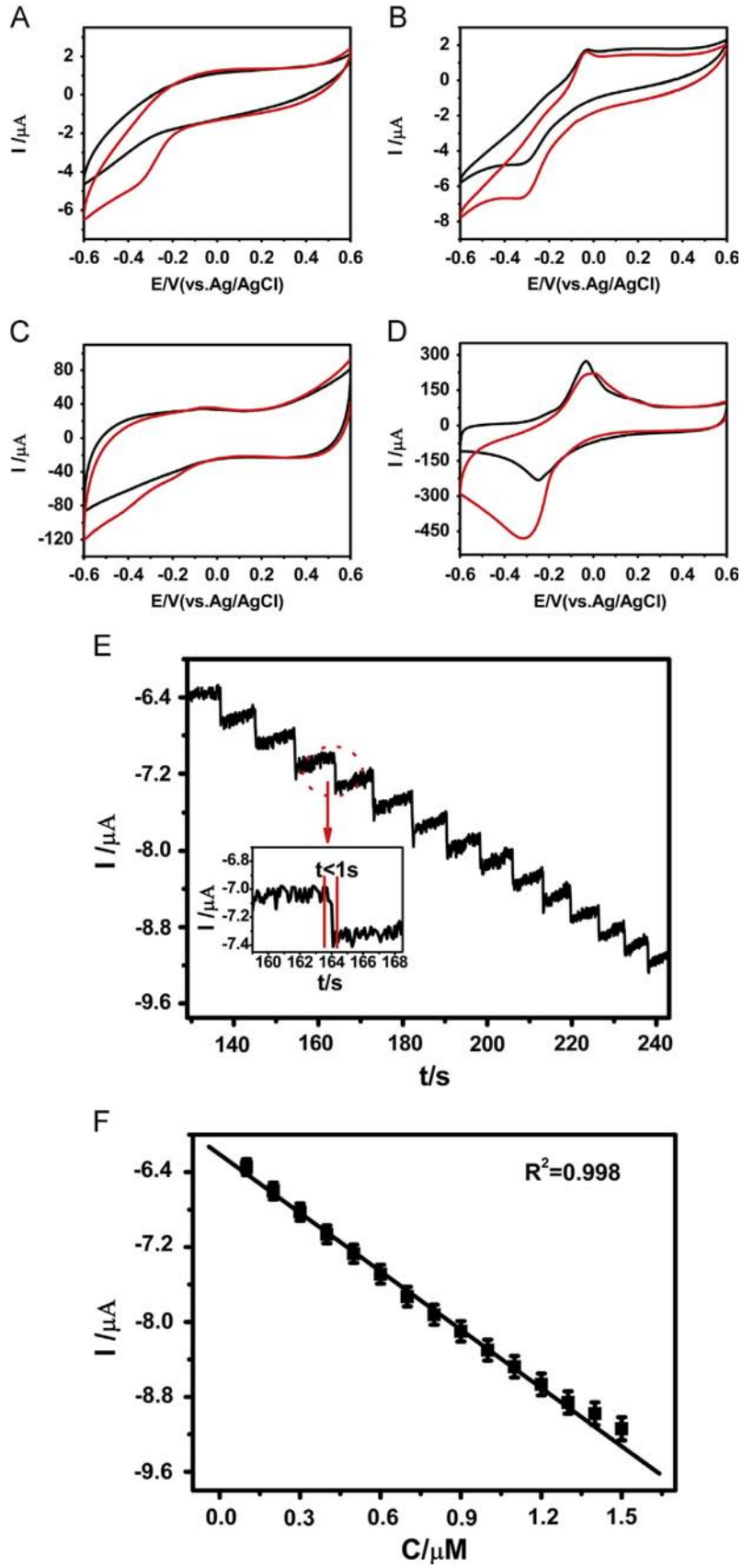

Fig. 6. (A) CVs of bare GCE (A), Cu-MOF/GCE (B), MPC/GCE (C), and Cu-MOF–MPC/GCE (D) in the absence (black line) and presence (red line) of 0.5 μM Hb in (pH=7.4). Scan rate: 50 mV s^{-1}. Starting potentials: 0.6 V. (E) Typical amperometric current–time curve of Cu-MOF–MPC/GCE with successive additions of Hb. Inset: the current response time after the Hb addition at Cu-MOF–MPC/GCE. (F) The linear dependence of between Hb concentration and current signal for Cu-MOF-MPC/GCE. (For interpretation of the references to color in this figure legend, the reader is referred to the web version of this article.)

retained. However, the crystalline structure of pure Cu-MOFs obviously deteriorated (Fig. 4D). These results show that the unstable redox property of Cu-MOFs is due to its instability in aqueous media. It is likely that Cu-MOFs and MPC interact to form new materials having homogenous structure and chemistry. MPC supports can enhance the water stability and thereby increase the electrochemical stability of Cu-MOFs.

3.2. Electrocatalysis of AA and Hb and their detection

In order to evaluate the electrochemical sensing properties of the as-prepared products, here the detection of AA and Hb is performed as electrochemical probe. CV measurements in the presence of 0.5 mM of AA were recorded for bare GCE, MPC/GCE, Cu-MOFs/GCE, and Cu-MOFs-MPC/GCE, which are shown in Fig. 5, respectively. Obviously, the bare GCE (Fig. 5A) and Cu-MOFs/GCE (Fig. 5B) display a weak electrocatalytic oxidation current toward AA. Furthermore, an obvious enhanced current response is observed for MPC/GCE (Fig. 5C). As compared to the bare GCE, MPC/GCE, and Cu-MOFs/GCE, a clear oxidation peak of AA appears at about +0.04 V for Cu-MOFs-MPC/GCE (Fig. 5D). Additionally, the oxidation current of AA at the Cu-MOFs-MPC/GCE exhibits an increased current signal, which is 4.2-, 7.0-, and 1.6-fold higher than that of the bare GCE, MPC/GCE, and Cu-MOFs/GCE, respectively. The results show that Cu-MOFs-MPC/GCE exhibits efficient catalytic activity toward the oxidation of AA. Thus, we focused on the investigation of the AA at the Cu-MOFs-MPC/GCE. Fig. 5E shows a typical amperometric current–time curve of Cu-MOFs-MPC/GCE with successive additions of AA. The best potential to be applied was chosen at +0.04 V based on the CVs measurements. Inset a of Fig. 5E shows the amperometric response of low concentration of AA at Cu-MOFs-MPC/GCE. This electrode responds very rapidly to the changes in the level of AA, producing steady-state signals less than 2 s (inset b of Fig. 5E). The relationship between AA concentration and current signal for Cu-MOFs-MPC/GCE is illustrated in Fig. 5F. The current increased linearly with the good linear ranges from 10 to 2360 μM (R^2=0.999, n=29) for AA detection with a sensitivity of 83.64 μA mM^{-1} and a detection limit of 3.5 μM (S/N=3). Error bars are the standard deviation of five repetitive experiments (RSD=3.9%). The RSD of current signal for 0.5 mM AA was less than 3.6% for five measurements for the same electrode. After being stored at 4 °C for 2 weeks, 8.2% current loss at Cu-MOFs-MPC/GCE was obtained by the amperometric response of 0.5 mM AA. The performance of the Cu-MOFs-MPC/GCE was also compared with other AA sensors (Table 1).

In Fig. 6, the CVs for Hb reduction at different electrodes were compared. Upon the addition 1 μM of Hb to the solution, it shows weak current response at bare GCE (Fig. 6A), Cu-MOFs/GCE (Fig. 6B), and MPC/GCE (Fig. 6C), respectively. However, an obvious enhancement of the peak current can be observed for Cu-MOFs-MPC/GCE (Fig. 6D) at −0.3 V. Obviously, the presence of Cu-MOFs-MPC/GCE made the electron transfer much easier compared with that of other as-prepared samples. This may have resulted from the macroporous structure of MPC with large surface area and unique nanocrystalline structure of Cu-MOFs. Thus, we focused on the investigation of the electrochemical properties of Cu-MOFs-MPC/GCE. Fig. 6E displays the current–time responses of Cu-MOFs-MPC/GCE for Hb detection with the applied potential of −0.3 V. The current response of Cu-MOFs-MPC/GCE generally reached a steady-state level within 1 s after the Hb addition (inset of Fig. 6E). The corresponding calibration plot for the reduction of Hb at Cu-MOFs-MPC/GCE was shown in Fig. 6F. Error bars are the standard deviation of five repetitive experiments (RSD=4.5%). The Hb sensor displays a linear range of 0.1 and 1.3 μM (R^2=0.998, n=13) with a sensitivity of 2077 μA mM^{-1}. The detection limit is calculated as 42 nM with the signal to noise ratio of three (S/N=3). The reproducibility of the sensor was also investigated by a current–time method for five repetitive measurements with additions of Hb concentration of 0.5 μM at −0.3 V. The RSD of the sensitivity was less than 3.2%. When the Cu-MOFs-MPC/GCE was stored at 4 °C for 2 weeks, the current response to 0.5 μM Hb remained 93.2% of its original value, suggesting the long-term stability of the modified electrode. The detailed comparison of Hb detection performance using different Hb electrochemical sensors is summarized in Table 2.

To evaluate the selectivity of the Cu-MOFs-MPC/GCE in the detection of AA and Hb, we investigated the influence of several compounds and ions that could serve as potential interferences in

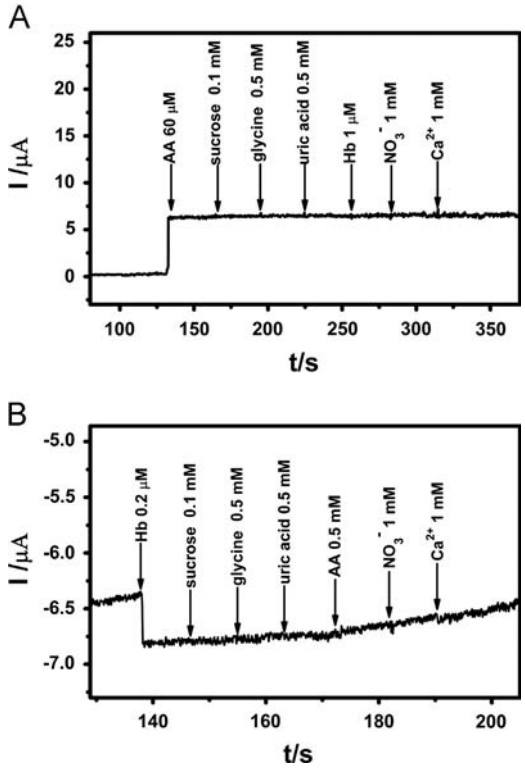

Fig. 7. *i–t* Curves of Cu-MOFs-MPC/GCE with addition of several possible interferences for AA (A) and Hb (B).

Table 2
Comparison of the performance of the Cu-MOFs-MPC/GCE for the electrochemical detection of Hb with that of other modified electrodes.

Working electrode	Potential (V)	Linear range	Sensitivity (μA mM^{-1})	Limit of detection (nM)	Reference
MB-MWNTs/GCE[a]	−0.3(Ag/AgCl)	5–2000 nM	579.5	1.5	[37]
bi-CoPc/DDAB/OMC/GCE[b]	−0.1(Ag/AgCl)	1–5 nM	–	–	[38]
C_{70}/DDAB/GCE[c]	−0.2 (Ag/AgCl)	20–200 μM	43.7	–	[39]
Cu-MOFs-MPC/GCE	−0.3 (Ag/AgCl)	0.1–1.3 μM	2077	42	This work

[a] Methylene blue-multiwalled carbon nanotubes nanohybrid-modified glassy carbon electrode.
[b] Binuclear cobalt phthalocyanine/surfactant/ordered mesoporous carbon modified glassy carbon electrode.
[c] Cationic surfacant didodecyldimethylammonium bromide containing C_{70} on a glassy carbon electrode.

the electrochemical experiments. Fig. 7A shows the current responses of the Cu-MOFs-MPC/GCE to AA and a series of possible interference. For 60 μM AA, an ignorable interference was observed for the following compounds and ions: sucrose, glycine, uric acid, Hb, NO^{3-} and Ca^{2+}. As can be seen from Fig. 7B, there is obvious current response with the addition of 0.2 μM Hb. On the contrary, no current response is observed with the addition of sucrose, glycine, uric acid, AA, NO^{3-} and Ca^{2+}. The results show good ability of anti-interference of the Cu-MOFs-MPC/GCE.

4. Conclusions

In conclusion, the thermal, water and electrochemical stability of Cu-MOFs and Cu-MOFs-MPC composites have been investigated. The morphology does not change after the immersion of Cu-MOFs-MPC in water for 2 h, verifying the good stability of this composite in aqueous media and further validating the subsequent studies on its electrochemical applications. Moreover, this composite displays excellent electrocatalytic ability for the reduction of Hb and oxidation of AA compared to the individual counterparts. As a result, the successful fabrication of Cu-MOFs-MPC not only promotes the development of the thermally, water and electrochemically stable porous composite materials, but also holds great promise for the design of biomolecular electrochemical sensors in neutral solution.

Acknowledgments

The authors gratefully acknowledge the financial support of the National Natural Science Foundation of China (No. 21075014) and the Fundamental Research Funds for the Central Universities (No. 12SSXT145).

References

[1] D.J. Tranchemontagne, J.L. Mendoza-Cortes, M. O'Keeffe, O.M. Yaghi, Chem. Soc. Rev. 38 (2009) 1257–1283.
[2] J.-P. Zhang, Y.-B. Zhang, J.-B. Lin, X.-M. Chen, Chem. Rev. 112 (2011) 1001–1033.
[3] M. Vallet-Regí, F. Balas, D. Arcos, Angew. Chem. Int. Ed. 46 (2007) 7548–7558.
[4] R.-Q. Zou, H. Sakurai, S. Han, R.-Q. Zhong, Q. Xu, J. Am. Chem. Soc. 129 (2007) 8402–8403.
[5] P. Horcajada, T. Chalati, C. Serre, B. Gillet, C. Sebrie, T. Baati, J.F. Eubank, D. Heurtaux, P. Clayette, C. Kreuz, J.S. Chang, Y.K. Hwang, V. Marsaud, P.N. Bories, L. Cynober, S. Gil, G. Férey, P. Couvreur, R. Gref, Nat. Mater. 9 (2010) 172–178.
[6] C. Liu, F. Li, L.-P. Ma, H.-M. Cheng, Adv. Mater. 22 (2010) E28–E62.
[7] R. Dawson, E. Stockel, J.R. Holst, D.J. Adams, A.I. Cooper, Energy Environ. Sci. 4 (2011) 4239–4245.
[8] L. Chen, K. Tan, Y.-Q. Lan, S.-L. Li, K.-Z. Shao, Z.-M. Su, Chem. Commun. 48 (2012) 5919–5921.
[9] G. Férey, F. Millange, M. Morcrette, C. Serre, M.-L. Doublet, J.-M. Grenèche, J.-M. Tarascon, Angew. Chem. Int. Ed. 46 (2007) 3259–3263.
[10] J. Zhao, F. Wang, P. Su, M. Li, J. Chen, Q. Yang, C. Li, J. Mater. Chem. 22 (2012) 13328–13333.
[11] J. Mao, L. Yang, P. Yu, X. Wei, L. Mao, Electrochem. Commun. 19 (2012) 29–31.
[12] R. Díaz, M.G. Orcajo, J.A. Botas, G. Calleja, J. Palma, Mater. Lett. 68 (2012) 126–128.
[13] D.Y. Lee, S.J. Yoon, N.K. Shrestha, S.-H. Lee, H. Ahn, S.-H. Han, Microporous Mesoporous Mater. 153 (2012) 163–165.
[14] K.F. Babu, M.A. Kulandainathan, I. Katsounaros, L. Rassaei, A.D. Burrows, P.R. Raithby, F. Marken, Electrochem. Commun. 12 (2010) 632–635.
[15] R. Senthil Kumar, S. Senthil Kumar, M. Anbu Kulandainathan, Electrochem. Commun. 25 (2012) 70–73.
[16] G. Jia, Y. Gao, W. Zhang, H. Wang, Z. Cao, C. Li, J. Liu, Electrochem. Commun. 34 (2013) 211–214.
[17] D.O. Miles, D. Jiang, A.D. Burrows, J.E. Halls, F. Marken, Electrochem. Commun. 27 (2013) 9–13.
[18] A. Morozan, F. Jaouen, Energy Environ. Sci. 5 (2012) 9269–9290.
[19] J.M. Taylor, R. Vaidhyanathan, S.S. Iremonger, G.K.H. Shimizu, J. Am. Chem. Soc. 134 (2012) 14338–14340.
[20] J.M. Taylor, K.W. Dawson, G.K.H. Shimizu, J. Am. Chem. Soc. 135 (2013) 1193–1196.
[21] H. Jasuja, N.C. Burtch, Y.-g. Huang, Y. Cai, K.S. Walton, Langmuir 29 (2012) 633–642.
[22] C. Petit, T.J. Bandosz, Adv. Mater. 21 (2009) 4753–4757.
[23] M. Jahan, Q. Bao, K.P. Loh, J. Am. Chem. Soc. 134 (2012) 6707–6713.
[24] P. Pachfule, B.K. Balan, S. Kurungot, R. Banerjee, Chem. Commun. 48 (2012) 2009–2011.
[25] Y. Zhang, X. Bo, C. Luhana, H. Wang, M. Li, L. Guo, Chem. Commun. 49 (2013) 6885–6887.
[26] Y. Zhang, L. Zeng, X. Bo, H. Wang, L. Guo, Anal. Chim. Acta 752 (2012) 45–52.
[27] W. Stober, A. Fink, E. Bohn, J. Colloid Interface Sci. 26 (1968) 62–69.
[28] S. Jun, J. Sang Hoon, R. Ryoo, M. Kruk, M. Jaroniec, Z. Liu, T. Ohsuna, O. Terasaki, J. Am. Chem. Soc. 122 (2000) 10712–10713.
[29] D. Sun, Y. Zhang, F. Wang, K. Wu, J. Chen, Y. Zhou, Sens. Actuators B 141 (2009) 641–645.
[30] C.-L. Sun, C.-T. Chang, H.-H. Lee, J. Zhou, J. Wang, T.-K. Sham, W.-F. Pong, ACS Nano 5 (2011) 7788–7795.
[31] C.-L. Sun, H.-H. Lee, J.-M. Yang, C.-C. Wu, Biosens. Bioelectron. 26 (2011) 3450–3455.
[32] W. Kit-Anan, A. Olarnwanich, C. Sriprachuabwong, C. Karuwan, A. Tuantranont, A. Wisitsoraat, W. Sriturayanich, A. Pimpin, J. Electroanal. Chem. 685 (2012) 72–78.
[33] R. Zhang, G.-D. Jin, D. Chen, X.-Y. Hu, Sens. Actuators B 138 (2009) 174–181.
[34] C. Xiao, X. Chu, Y. Yang, X. Li, X. Zhang, J. Chen, Biosens. Bioelectron. 26 (2011) 2934–2939.
[35] S. Zhu, H. Li, W. Niu, G. Xu, Biosens. Bioelectron. 25 (2009) 940–943.
[36] M. Noroozifar, M. Khorasani-Motlagh, R. Akbari, M. Bemanadi Parizi, Biosens. Bioelectron. 28 (2011) 56–63.
[37] S. Pakapongpan, R. Palangsuntikul, W. Surareungchai, Electrochim. Acta 56 (2011) 6831–6836.
[38] L. Liu, L.-p. Guo, X.-j. Bo, J. Bai, X.-j. Cui, Anal. Chim. Acta 673 (2010) 88–94.
[39] M. Li, M. Xu, N. Li, Z. Gu, X. Zhou, J. Phys. Chem. B 106 (2002) 4197–4202.